ADVANCED FUNCTIONAL MATERIALS
www.afm-journal.de

Robust Memristive Fiber for Woven Textile Memristor

Yue Liu, Xufeng Zhou, Hui Yan, Zhengfeng Zhu, Xiang Shi, Yahui Peng, Lin Chen, Peining Chen, and Huisheng Peng**

Memristors with an intrinsic crossbar structure and high computing capability offer promising opportunities for the flexible information-processing component that can well integrate with the interwoven structure of electronic textiles. However, it remains difficult to achieve uniform inorganic memristive layer at nanometer thickness on the curved surface of fiber electrode, thus hindering the applications of textile memristors. Here, a high-performing and reliable textile memristor made of robust Pt/$CsPbBr_3$ fiber through an electric-field-assisted assembly method is reported. The textile memristor exhibits a cycle to cycle variation of less than 8% and an average set voltage of ≈0.16 V, which is lower than that of the majority of planar metal-oxide memristors. The flexible and mechanically robust Pt/$CsPbBr_3$ fibers are woven into a scalable textile memristor array with good device-to-device reproducibility. This textile memristor can be seamlessly integrated with textile electronics toward a smart clothes system to accurately process complicated physiological information, providing an effective interactive interface for intelligent healthcare.

1. Introduction

Electronic textiles capable of sensing,[1,2] supplying electricity,[3,4] and displaying[5,6] are empowering various fields of smart engineering for flexible electronics, information technologies, and biomedical applications.[7,8] Among them, information-processing component is the indispensable building block to transmit, store and/or process the data from other functional components. However, conventional planar information-processing devices that are attached to the textile are typically based on rigid planar substrates and require complex electrical connections for complete circuit.[5,9] As a result, the surface roughness and complex deformation of textiles generally degrade or even disable the attached devices, and in turn, the devices inevitably diminish the flexibility and breathability of textiles. Designing scalable information-processing devices having the interwoven architecture that well unifies with textile fabrication is urgently needed but far less developed.

With an intrinsic crossbar structure compatible with textile and excellent computing capabilities, memristor is considered as a suitable component to fabricate textile information-processing system by replacing planar electrodes with flexible fiber ones.[10,11] To achieve efficient conductive filaments and ion transport, it is critical to deposit uniform nanometer-thick active layer—typically made of inorganic materials[12–14]—onto flexible conductive fiber electrodes. While high-quality inorganic memristive film could be achieved through methods of physical vapor deposition, chemical vapor deposition or spin coating that are widely used in planar electronic devices, they are hardly applicable to one-dimensional fiber electrodes having a curved surface.[15,16] Most recently, dip coating and electrochemical deposition were typically used to load inorganic active materials on fiber electrodes,[17–19] but difficult to achieve smooth memristive layer that requires both high evenness and ultrathin thickness at nanometer scale. Fabricating flexible and robust functional fibers with uniform inorganic memristive layer at the nanometer scale remains an unmet need to realize a high-performing textile memristor.

Herein, we report a high-performing textile memristor made of flexible fiber electrode with uniform memristive layer at nanometer scale through an electric-field-assisted (EFA) assembly method (**Figure 1**a). Using such an EFA assembly method, the memristive inorganic materials such as TiO_2, ZnO, and $CsPbBr_3$ quantum dot were continuously and uniformly deposited on the fiber electrode with an accurate tunability. As a demonstration, the resultant textile memristor weaving with Pt/$CsPbBr_3$ fiber exhibited a low set voltage (≈0.16 V), long retention time (>5000 s), high on/off ratio (>10^5) and switching uniformity (set voltage variation of <8%). Such a memristor was also flexible and mechanically stable to withstand over 1000 cycles of bending. The woven textile memristor array containing 49 working units showed good device-to-device reproducibility, thus promising to realize real-time health monitoring electronic textiles for patients with arrhythmia disease.

Y. Liu, X. Zhou, Z. Zhu, X. Shi, P. Chen, H. Peng
State Key Laboratory of Molecular Engineering of Polymers
Laboratory of Advanced Materials and
Department of Macromolecular Science
Fudan University
Shanghai 200438, P. R. China
E-mail: peiningc@fudan.edu.cn; penghs@fudan.edu.cn
H. Yan, Y. Peng
School of Electronic and Information Engineering
Beijing Jiaotong University
Beijing 100044, P. R. China
L. Chen
State Key Laboratory of ASIC and System
School of Microelectronics
Fudan University
Shanghai 200433, P. R. China

The ORCID identification number(s) for the author(s) of this article can be found under https://doi.org/10.1002/adfm.202201510.

DOI: 10.1002/adfm.202201510

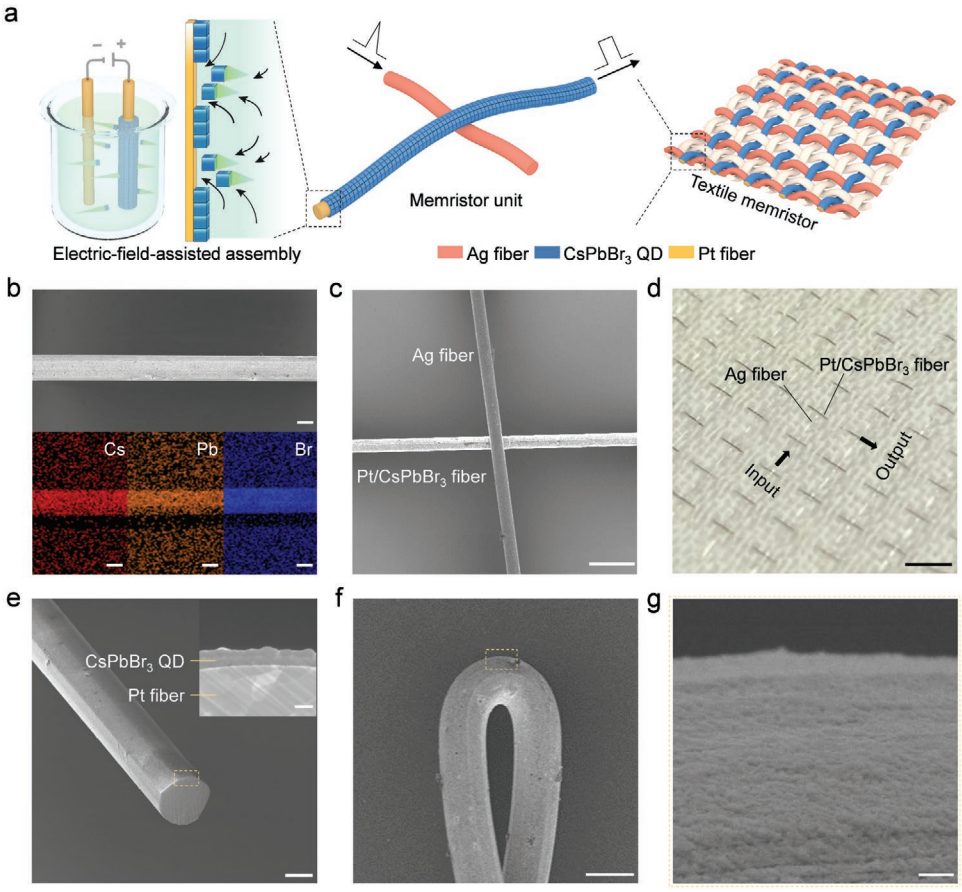

Figure 1. $Pt/CsPbBr_3$ fiber and textile memristor. a) Schematic of fabrication process of textile memristor using $Pt/CsPbBr_3$ fibers through EFA assembly method. b) Scanning electron microscopy (SEM) (top) and energy-dispersive X-ray spectroscopy (bottom) images of $Pt/CsPbBr_3$ fiber. c) SEM image of a textile memristor unit made from interlaced Ag and $Pt/CsPbBr_3$ fiber. d) Photograph of a textile memristor consisting of 49 memristor units. e) Cross-sectional SEM image of $Pt/CsPbBr_3$ fiber and its enlarged view (top right inset). f) SEM image of a bent $Pt/CsPbBr_3$ fiber with bending radius of 20 µm. g) Enlarged SEM image of surface of $Pt/CsPbBr_3$ fiber as marked with yellow dotted box in (f). Scale bars: 10 µm (b), 100 µm (c), 3 mm (d), 10 µm (e), 200 nm (inset of (e)), 20 µm (f), 200 nm (g).

2. Results and Discussion

Through electric-field-assisted (EFA) assembly method, uniform and thickness-tunable active materials could be effectively deposited onto conductive substrates with various sizes and shapes driven by electric field.[20–22] Thus such a method is potentially suitable to effectively load active layer on fiber substrate with a curved surface. We chose $CsPbBr_3$ quantum dot (QD) as the building block to assemble memristive layer in this study because it has high ionic conductivity and structural stability for superior resistive switching performance and durability.[23–25] For a typical $CsPbBr_3$ memristor, due to the highly active Br ions in $CsPbBr_3$ layer, conductive Br vacancies can be formed under external voltage, thus enabling resistive switching.[26,27] $CsPbBr_3$ QD was first synthesized by a triple-ligands method at room temperature (see details in the Experimental Section),[28] which was confirmed by X-ray diffraction pattern (Figure S1, Supporting Information). The $CsPbBr_3$ QD demonstrated a typical cubic crystal morphology with a uniform size of 12 ± 2.68 nm (Figure S2, Supporting Information), and could be stably dispersed in n-octane solution for over 20 days (Figure S3, Supporting Information). The $CsPbBr_3$ QD had a negatively-charged surface from the negative zeta potential of −37.4 mV, which originated from the rich distribution of Br ions on its surface.[25,29] Such uniform cubic morphology and negatively-charged surface of $CsPbBr_3$ QD were helpful for its compact and uniform arrangement on the fiber substrate during the assembly process.

In a typical EFA assembly process (Figure 1a), two Pt fiber electrodes were parallelly placed into the $CsPbBr_3$ QD solution. When a voltage was applied to the electrodes, the negatively-charged surface enabled $CsPbBr_3$ QD to migrate toward the positive fiber electrode to form $CsPbBr_3$ film.[21] The resultant $Pt/CsPbBr_3$ fibers could be woven with Ag fibers to form a textile memristor, where each interlaced point functions as an individual memristor unit (Figure 1b–d; Figure S4, Supporting Information). The thickness and quality of $CsPbBr_3$ film could be accurately tuned in a facile way by changing the concentration of $CsPbBr_3$ QD solution, applied voltage and/or depositing time (Figure S5, Supporting Information). We traced the depositing process under different conditions and found that the $CsPbBr_3$ QD preferentially deposited on the exposed areas on the Pt fiber, and eventually filled the remaining pores to form a dense and even $CsPbBr_3$ layer (Figure S5, Supporting

Information). A fiber electrode having an optimized $CsPbBr_3$ film with a thickness of ≈200 nm was demonstrated in Figure 1e. The Pt fiber was fully covered with $CsPbBr_3$ QD without any obvious pinholes, where the characteristic elements of Cs, Pb, and Br were homogenously distributed from the energy-dispersive X-ray spectroscopy analysis (Figure 1b; Figure S6, Supporting Information). The $CsPbBr_3$ film had a smooth surface with a small average roughness factor of 6.6 nm (Figure S7, Supporting Information). Moreover, the EFA assembly method could be generalized to evenly deposit other common inorganic memristive materials like TiO_2 and ZnO onto various conductive fibers with a wide range of diameters from 20 to 130 µm (Figures S8–S10, Supporting Information).

Statistical analysis verified that the fiber electrode (with a length of 5 cm) was fully covered with $CsPbBr_3$ QD along the length direction, and in particular, such a full coverage of $CsPbBr_3$ was well repeatable for multiple batches of Pt fibers (Figure S11, Supporting Information), indicating high reproducibility of the EFA assembly method. Such spatial uniformity of $CsPbBr_3$ QD at different positions on the fiber electrodes could ensure the stability of the resultant textile memristor for wearable use. We further evaluated the mechanical stability and flexibility of Pt/$CsPbBr_3$ fiber. No obvious cracks on the film were observed when the Pt/$CsPbBr_3$ fiber was bent at a curvature radius of 20 µm (Figure 1f,g; Figure S12, Supporting Information), which was indicative of robustness and reliability of the memristive layer, and crucial to the stability of resultant textile memristor to withstand various deformations in practical wearable applications.

In comparison, by using dip coating method that is commonly used to load active materials onto the fiber electrode, uneven distribution of $CsPbBr_3$ QD with lots of holes was obviously observed even after over 100 times of dip-coating operations (Figures S13 and S14, Supporting Information). The average roughness factor (17 nm) of the surface of $CsPbBr_3$ layer was 2.5 times higher than that using EFA assembly method. Based on the detailed analysis of film quality with dip-coating times, QD tended to aggregate with each other to form large particles. Statistical analysis indeed indicated that nearly 20% of the surface area on the fiber electrode was exposed without any coverage of $CsPbBr_3$ QD, and the coverage ratio of $CsPbBr_3$ QD largely fluctuated from 40% to 80% along the length direction and for different batches of Pt fibers. The uneven and incomplete coverage was mainly attributed to the redissolution and aggregation of $CsPbBr_3$ QD during the repeated dip-coating operations.[30,31]

The prepared Pt/$CsPbBr_3$ fiber was interlaced with an Ag fiber to fabricate a textile memristor unit (Figure 1c). The electrical measurements of the textile memristor unit were performed by applying a direct voltage sweep to the Ag working electrode and Pt/$CsPbBr_3$ fiber (**Figure 2**a). Inherited from the high-quality $CsPbBr_3$ memristive layer on the fiber electrode through EFA assembly method, the textile memristor unit exhibited robust comprehensive electrical performances. For instance, the current–voltage (I–V) curves indicated that the textile memristor unit had a low average set voltage of ≈0.16 V with slight variations in the investigated 50 switching cycles (Figure 2b). Such set voltage is lower than that for the majority of metal-oxide memristors.[32–34] The resistances of both high resistance state (HRS) and low resistance state (LRS) for the memristor unit were well maintained in the repeated switching cycles (Figure 2c), accompanied by a high resistance ratio (>10^5) of HRS to LRS. In addition, as shown in Figure 2d, four discrete LRS states from 10^2 to 10^4 Ω were readily tuned by changing the compliance currents. Such memristor with multiple resistance states is desired to achieve multi-level memory.

We further made detailed comparisons of memristive performances for textile memristors based on different deposition methods. The set voltage of textile memristor prepared by EFA assembly method was well maintained with a small fluctuation of less than 8% (Figure 2e). In comparison, the textile memristor using dip-coated fiber showed anomalous variation in the I–V curves (Figure S15, Supporting Information), where the set voltage largely fluctuated by over 13%. In addition, the resistance of HRS largely fluctuated from 10^8 to 10^{12} Ω in an operating duration of 5000 s (Figure 2f), compared with the stably-maintained values of textile memristor based on EFA assembly method. These comparison results showed that EFA assembly method endowed fiber electrode with high-quality memristive layer, thus enabling textile memristor to have good cycle-to-cycle uniformity and retention reliability.

The performing stability and durability of textile memristor under complex deformations are crucial to practical wearable use. We first evaluated the electrical performances of a woven textile memristor unit under bending, and did not observe any obvious variation in both HRS and LRS when the textile (with a size of 2 × 5 cm^2) was repeatedly bent for 1000 cycles (with a bending radius of 20 mm, Figure 2g; Figures S16 and S17, Supporting Information). Moreover, due to the uniformity of $CsPbBr_3$ memristive layer on the curved surface of fiber electrode, the resistance values of HRS and LRS were well maintained when the Ag fiber interlaced with Pt/$CsPbBr_3$ fiber at different positions along both length and circumferential directions (Figure 2h; Figures S18 and S19, Supporting Information), enabling the textile memristor working stably after sliding over each other between crossed two fiber electrodes that caused by textile deformations. In addition, the electrical performance of our textile memristor remained almost unchanged after it was stored in the ambient environment for 20 days (Figure S20, Supporting Information). Overall, due to the mechanical robustness and environmental reliability of $CsPbBr_3$ film through EFA assembly method, our textile memristor is stable and durable to withstand various harsh conditions in practical wearable applications.

Scalable textile memristor array was further fabricated by weaving multiple Ag fibers, Pt/$CsPbBr_3$ fibers and commercial polymer fibers together, in which the interlaced points between Ag and Pt/$CsPbBr_3$ fibers worked as memristor units (**Figure 3**a). For a textile memristor containing 49 memristor units (7 × 7 array, Figure 3b), the I–V curves of each unit based on EFA assembly method showed repeatable switching performances with a small set voltage variation of 10% (Figure 3c). Such textile memristor units also had a high device yield of 96% (Figure 3d), indicating good device-to-device reproducibility. In comparison, most textile memristor units based on dip-coating method were disabled, with a much lower device yield of 39%, and even the remaining working units showed largely-varied switching behaviors (Figure 3e). As expected, the textile memristor units prepared by EFA assembly showed a much narrower distribution of set voltage and resistance state compared

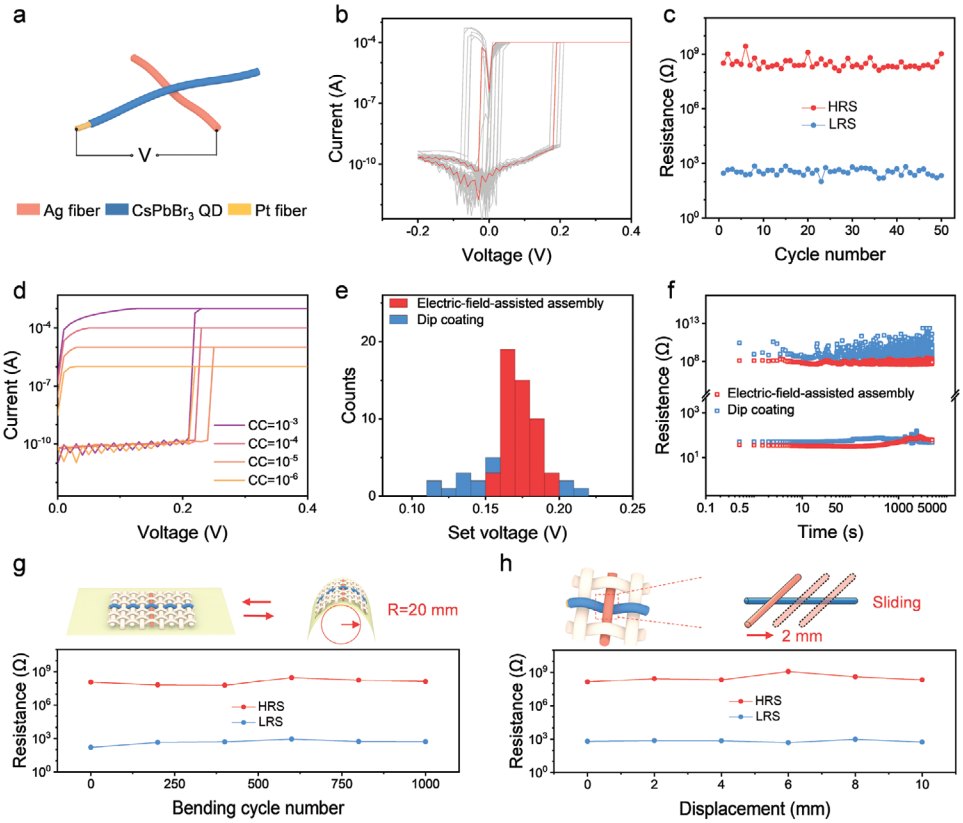

Figure 2. Memristive characteristics and stability of textile memristor unit. a) Schematic of a textile memristor unit for electrical characteristic measurement. b) Current–voltage curves of memristor using Pt/$CsPbBr_3$ fiber by EFA assembly method as applied with 50 consecutive voltage sweeps. c) The resistance values of high resistance state (HRS) and low resistance state (LRS) during 50 switching cycles. d) Resistive switching behavior of memristor with different compliance currents (CC). e) Set voltage distribution and f) retention time of memristor using Pt/$CsPbBr_3$ fiber by EFA assembly and dip coating methods. g) HRS and LRS values as the memristor unit woven in a textile was repeatedly bent at a curvature radius of 20 mm. h) HRS and LRS values as the Ag fiber electrode slid on the Pt/$CsPbBr_3$ fiber with different displacements.

with that based on dip-coating method (Figure 3f; Figure S21, Supporting Information). Together, these results indicated that the textile memristor array prepared by EFA assembly had good device-to-device reproducibility and is promising for large-scale fabrication and application.

The data-processing capability of our textile memristor was then evaluated through a typical simulation based on the measured characteristics (Figure S22, Supporting Information). Our textile memristor could efficiently and correctly perform information-processing tasks. For instance, as a typical recognizing model, a three-layer artificial neural network with 784 input neurons, 300 hidden neurons and 10 output neurons was designed to recognize the Modified National Institute of Standards and Technology (MNIST) handwritten dataset images (**Figure 4**a).[35–37] After only 15 learning epochs of 60 000 images, an average recognition accuracy of 87% was achieved by a textile memristor after testing 10 000 images (Figure 4b). The confusion matrix showed that each digit image was optimally recognized, which was reliable enough for further learning and recognizing applications.[38,39]

Smart electronic textile is considered as one ultimate form of wearables to bridge human-machine interaction.[5,40] As a proof-of-concept, we demonstrated our textile memristor integrated into a smart clothes could serve as a real-time diagnosis tool for personalized healthcare by processing complicated physiological information like electrocardiogram signal (ECG) patterns collected from patients with arrhythmia diseases, enabling the classification of five distinct health states (Figure 4c; Table S1, Supporting Information).[41–43] Specifically, these collected ECG signals were converted to specific voltage pulses to input into the artificial neural network based on textile memristor units. Different weight values were repeatedly output by comparing with the ideal values, so as to update to form minimum errors through the back-propagation algorithm with increasing learning epochs. After only 15 epochs, the weight values of each class exhibited recognizable waveforms and morphologies with a high final classify accuracy of 83% (Figure 4d,e), indicating that the characteristic ECG had been accurately processed. With these data processing capabilities, it is envisioned that our textile memristor array can integrate with other electronic textiles to realize real-time health monitoring and treatment without professional training, especially for the elderly living alone.

3. Conclusion

In summary, an efficient and facile electric-field-assisted assembly method was employed to prepare uniform and robust memristive layer on fiber electrode for textile memristor. The

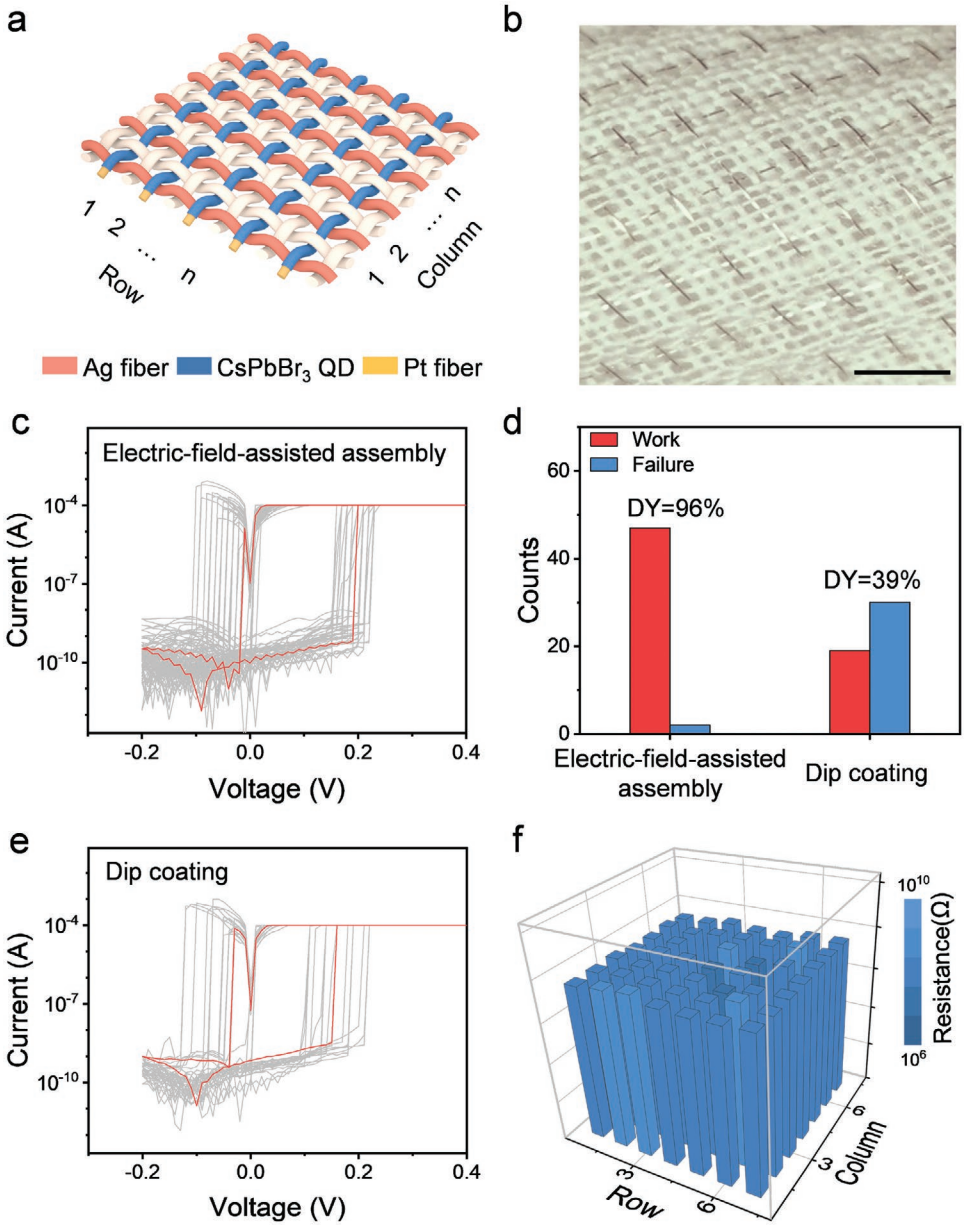

Figure 3. Memristive characteristics of textile memristor array. a,b) Schematic and photograph of textile memristor array, respectively. Scale bar in (b) is 3 mm. c) Current–voltage curves of a textile memristor array containing 49 memristor units using fibers by EFA assembly method. d) Device yield (DY) of textile memristor array using fibers based on EFA assembly and dip coating methods. e) Current–voltage curves of a textile memristor array containing 49 memristor units using fibers based on dip coating method. f) The HRS resistance distribution of textile memristor array using fibers prepared by EFA assembly method.

resultant textile memristor array woven by Pt/$CsPbBr_3$ fibers exhibited a low set voltage (≈0.16 V), high cycle-to-cycle uniformity and good device-to-device reproducibility, which will effectively unlock the development of the flexible information-processing system that is well integrated with electronic textiles. Our scalable textile memristor array could potentially function as a real-time diagnosis tool by processing complicated physiological information like electrocardiogram signals with high recognition accuracy. With the integration of sensing, displaying, and supplying electricity, the textile memristor is poised to offer exciting opportunities for multi-functional smart textile systems.

4. Experimental Section

Materials: $PbBr_2$ (99.999%), Cs_2CO_3 (99.9%), and didodecyldimethylammonium bromide (DDAB, 98%) were purchased from Aladdin. Octanoic acid (OTAc, 99%) and tetraoctylammonium bromide (TOAB, 98%) were purchased from Macklin Inc. Toluene (99.5%) and ethyl acetate (99.5%) were obtained from Sigma-Aldrich. Ag fibers (99.99%, with a diameter of 20 µm) and Pt fibers (99.99%, with diameters of 20, 50, and 100 µm) were ordered from Alfa Aesar. These materials were used as received without further treatment.

Synthesis of $CsPbBr_3$ QD Solution: A room-temperature triple-ligands method was used to synthesize $CsPbBr_3$ QD solution.[26] First, 1.5 mL of cesium precursor solution (1 mM Cs_2CO_3 in OTAc) was quickly

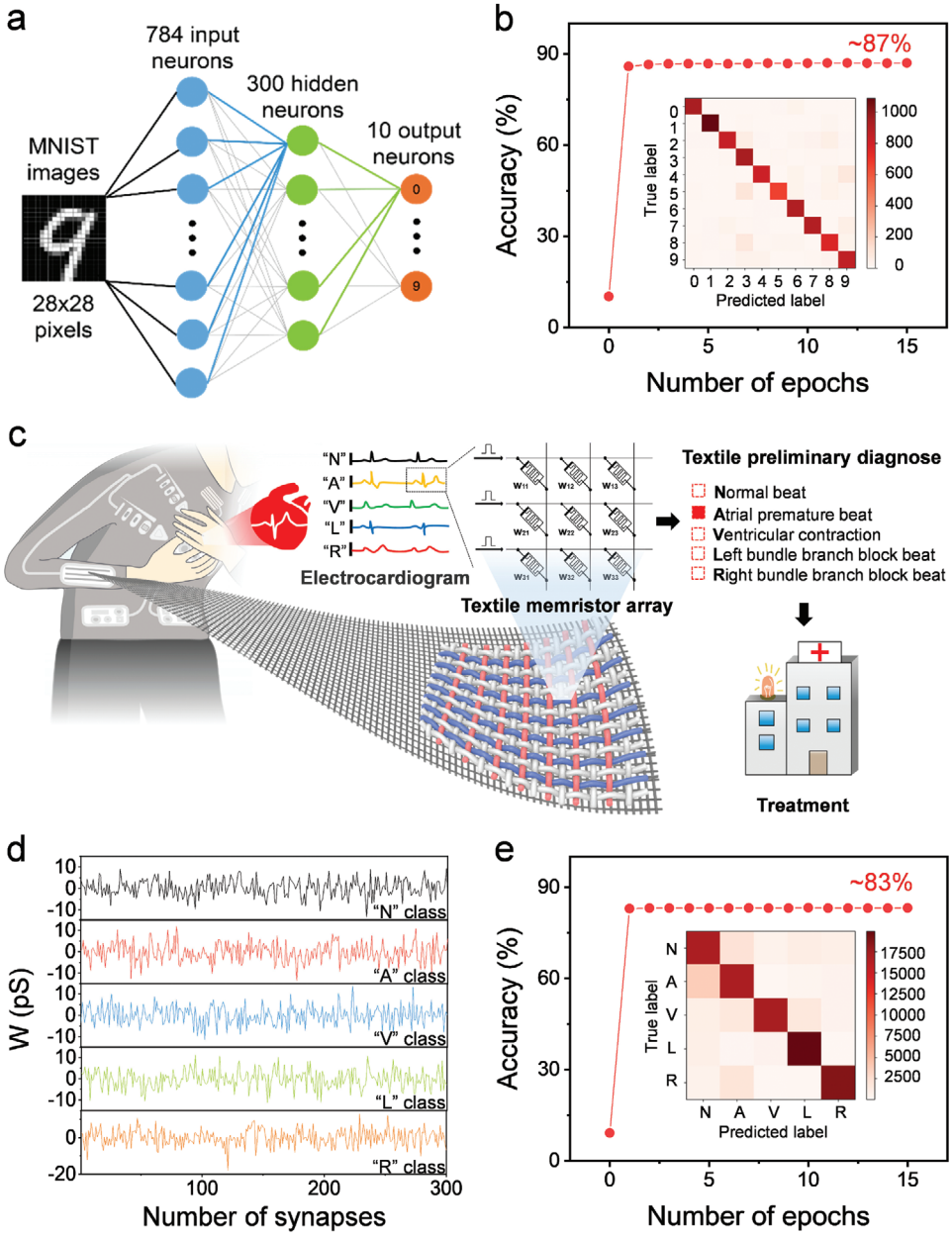

Figure 4. Processing capacity of textile memristor to recognize MNIST images and ECG patterns. a) Schematic of a three-layer neural network. b) Recognition accuracy evolution with learning epochs for MNIST images and confusion matrix that compared predicted label with true label (inset). c) Schematic of smart healthcare clothes integrated with textile memristor as information-processing component to analyze physiological information and display the categorizing results. d) Featured weight values of each class connected to the output neuron after learning process. e) Recognition accuracy for ECG patterns corresponding to learning epochs and confusion matrix that compared predicted label with true label (inset).

added into 6 mL of $PbBr_2$ solution (1 mM $PbBr_2$ and 2 mM TOAB in toluene). The reaction mixture was stirred for 5 min in open air. 1 mL of DDAB solution (in toluene 10 mg·mL^{-1}) was then injected into the above mixture, followed by stirring for 2 min. To purify, extra ethyl acetate was added into the QD crude solution with a volume ratio of 2:1. After centrifuging at a rate of 6000 revolutions per minute for 3 min, the precipitate was collected and dispersed in *n*-octane for further use.

Fabrication of Pt/CsPbBr$_3$ Fiber: Two Pt fibers serving as positive and negative electrodes were immersed in as-synthesized $CsPbBr_3$ QD solution, spaced at approximately 5 mm from each other. The EFA assembly process was then performed under a direct voltage. The morphology and thickness of $CsPbBr_3$ QD film could be controlled by the concentration of $CsPbBr_3$ QD solution, applied voltage and time during the process. After optimization, the $CsPbBr_3$ QD was deposited on the positive Pt electrode under a voltage of 40 V for 10 min in QD solution (with a concentration of 1 mg mL^{-1}). Finally, the Pt/$CsPbBr_3$ fiber was dried at room temperature before testing.

Preparation of Textile Memristor: The multiple Ag fibers as working electrodes were carefully woven with the Pt/$CsPbBr_3$ fibers to fabricate textile memristor. To measure the electrical performance of memristor, the working electrode was connected with semiconductor characterization system to supply external bias, while the Pt fiber as counter electrode was grounded.

Characterization: The chemical properties of $CsPbBr_3$ QD were characterized by transmission electron microscopy (TEM, JEOL JEM-2100F operated at 200 kV), X-ray diffraction (Bruker AXSD8) and dynamic light scattering detector (Malvern-Nano ZS90). The morphologies of $CsPbBr_3$ film were analyzed through field emission scanning electron microscopy (SEM, Zeiss Gemini SEM500 FESEM operated at 5 kV; EDS, Aztec X-Max Extreme EDS operated at 10 kV) and atomic force microscopy (Fast-scan module). The coverage ratio of $CsPbBr_3$ film on the Pt fiber electrode was calculated by the different brightness between coverage and exposed electrode through Image J analysis. The photographs were captured by a digital camera (Sony A6000, Japan). The electrical measurements of the memristor were performed by Keithley 2400 and 2612 Source Meter.

Simulation: The artificial neural network simulation was performed on the tool of platform CrossSim.[44] A three-layer fully connected neural network was utilized to perform supervised learning with the pre-processed MNIST images and ECG patterns datasets, based on back-propagation algorithm.

Statistical Analysis: The set voltage variation is defined as the standard deviation of set voltage divided by its average value. The particle size of $CsPbBr_3$ QD was presented as the mean ± standard deviation of total QD particle sizes in TEM image.

Supporting Information

Supporting Information is available from the Wiley Online Library or from the author.

Acknowledgements

Y.L. and X.Z. contributed equally to this work. This work was supported by NSFC (22175042), STCSM (20JC1414902, 21511104900, 19QA1400800) and SHMEC (2017-01-07-00-07-E00062). Part of the sample fabrication was performed at the Fudan Nano-fabrication Laboratory.

Conflict of Interest

The authors declare no conflict of interest.

Data Availability Statement

The data that support the findings of this study are available from the corresponding author upon reasonable request.

Keywords

$CsPbBr_3$ quantum dots, electric-field-assisted assemblies, electronic textiles, memristors

Received: February 7, 2022
Revised: March 17, 2022
Published online: April 10, 2022

[1] C. Wan, G. Chen, Y. Fu, M. Wang, N. Matsuhisa, S. Pan, L. Pan, H. Yang, Q. Wan, L. Zhu, X. Chen, *Adv. Mater.* **2018**, *30*, 1801291.
[2] F. Guan, Y. Xie, H. Wu, Y. Meng, Y. Shi, M. Gao, Z. Zhang, S. Chen, Y. Chen, H. Wang, Q. Pei, *ACS Nano* **2020**, *14*, 15428.
[3] G. Chen, Y. Li, M. Bick, J. Chen, *Chem. Rev.* **2020**, *120*, 3668.
[4] Y. Gong, K. Fu, S. Xu, J. Dai, T. R. Hamann, L. Zhang, G. T. Hitz, Z. Fu, Z. Ma, D. W. McOwen, X. Han, L. Hu, E. D. Wachsman, *Mater. Today* **2018**, *21*, 594.
[5] X. Shi, Y. Zuo, P. Zhai, J. Shen, Y. Yang, Z. Gao, M. Liao, J. Wu, J. Wang, X. Xu, Q. Tong, B. Zhang, B. Wang, X. Sun, L. Zhang, Q. Pei, D. Jin, P. Chen, H. Peng, *Nature* **2021**, *591*, 240.
[6] G. Liang, M. Yi, H. Hu, K. Ding, L. Wang, H. Zeng, J. Tang, L. Liao, C. Nan, Y. He, C. Ye, *Adv. Electron. Mater.* **2017**, *3*, 1700401.
[7] J. S. Heo, J. Eom, Y. H. Kim, S. K. Park, *Small* **2018**, *14*, 1703034.
[8] W. Zeng, L. Shu, Q. Li, S. Chen, F. Wang, X. Tao, *Adv. Mater.* **2014**, *26*, 5310.
[9] Z. Zhou, K. Chen, X. Li, S. Zhang, Y. Wu, Y. Zhou, K. Meng, C. Sun, Q. He, W. Fan, E. Fan, Z. Lin, X. Tan, W. Deng, J. Yang, J. Chen, *Nat. Electron.* **2020**, *3*, 571.
[10] X. Xu, X. Zhou, T. Wang, X. Shi, Y. Liu, Y. Zuo, L. Xu, M. Wang, X. Hu, X. Yang, J. Chen, X. Yang, L. Chen, P. Chen, H. Peng, *Angew. Chem., Int. Ed.* **2020**, *59*, 12762.
[11] T. Wang, J. Meng, M. Rao, Z. He, L. Chen, H. Zhu, Q. Sun, S. Ding, W. Bao, P. Zhou, D. W. Zhang, *Nano Lett.* **2020**, *20*, 4111.
[12] X. Yan, Y. Pei, H. Chen, J. Zhao, Z. Zhou, H. Wang, L. Zhang, J. Wang, X. Li, C. Qin, G. Wang, Z. Xiao, Q. Zhao, K. Wang, H. Li, D. Ren, Q. Liu, H. Zhou, J. Chen, P. Zhou, *Adv. Mater.* **2019**, *31*, 1805284.
[13] Q. Xia, J. J. Yang, *Nat. Mater.* **2019**, *18*, 309.
[14] Z. Wang, H. Wu, G. W. Burr, C. S. Hwang, K. L. Wang, Q. Xia, J. J. Yang, *Nat. Rev. Mater.* **2020**, *5*, 173.
[15] S. Pi, C. Li, H. Jiang, W. Xia, H. Xin, J. J. Yang, Q. Xia, *Nat. Nanotechnol.* **2019**, *14*, 35.
[16] D. Wang, Y. Dai, J. Xu, L. Chen, Q. Sun, P. Zhou, P. Wang, S. Ding, D. W. Zhang, *IEEE Electron Device Lett.* **2016**, *37*, 878.
[17] J. He, C. Lu, H. Jiang, F. Han, X. Shi, J. Wu, L. Wang, T. Chen, J. Wang, Y. Zhang, H. Yang, G. Zhang, X. Sun, B. Wang, P. Chen, Y. Wang, Y. Xia, H. Peng, *Nature* **2021**, *597*, 57.
[18] D. Kang, T. W. Kim, S. R. Kubota, A. C. Cardiel, H. G. Cha, K. S. Choi, *Chem. Rev.* **2015**, *115*, 12839.
[19] L. Xu, X. Fu, F. Liu, X. Shi, X. Zhou, M. Liao, C. Chen, F. Xu, B. Wang, B. Zhang, H. Peng, *J. Mater. Chem. A* **2020**, *8*, 5476.
[20] K. W. Song, R. Costi, V. Bulović, *Adv. Mater.* **2013**, *25*, 1420.
[21] Y. Yu, D. Yu, C. A. Orme, *Nano Lett.* **2017**, *17*, 3862.
[22] Y. Yu, D. Yu, B. Sadigh, C. A. Orme, *Nat. Commun.* **2018**, *9*, 4211.
[23] L. Xu, J. Li, T. Fang, Y. Zhao, S. Yuan, Y. Dong, J. Song, *Nanoscale Adv.* **2019**, *1*, 980.
[24] Y. Wu, Y. Wei, Y. Huang, F. Cao, D. Yu, X. Li, H. Zeng, *Nano Res.* **2017**, *10*, 1584.
[25] X. Li, F. Cao, D. Yu, J. Chen, Z. Sun, Y. Shen, Y. Zhu, L. Wang, Y. Wei, Y. Wu, H. Zeng, *Small* **2017**, *13*, 1603996.
[26] D. Liu, Q. Lin, Z. Zang, M. Wang, P. Wangyang, X. Tang, M. Zhou, W. Hu, *ACS Appl. Mater. Interfaces* **2017**, *9*, 6171.
[27] Y. Wang, Z. Lv, Q. Liao, H. Shan, J. Chen, Y. Zhou, L. Zhou, X. Chen, V. A. L. Roy, Z. Wang, Z. Xu, Y. Zeng, S. Han, *Adv. Mater.* **2018**, *30*, 1800327.
[28] J. Song, J. Li, L. Xu, J. Li, F. Zhang, B. Han, Q. Shan, H. Zeng, *Adv. Mater.* **2018**, *30*, 1800764.
[29] X. Jin, X. Zhang, H. Fang, W. Deng, X. Xu, J. Jie, X. Zhang, *Adv. Funct. Mater.* **2018**, *28*, 1705189.
[30] H. Uchiyama, D. Shimaoka, H. Kozuka, *Soft Matter* **2012**, *8*, 11318.
[31] X. Tang, X. Yan, *J. Sol-Gel. Sci. Technol.* **2017**, *81*, 378.
[32] D. Wang, L. Wang, W. Ran, S. Zhao, R. Yin, Y. Yan, K. Jiang, Z. Lou, G. Shen, *Nano Energy* **2020**, *76*, 105109.
[33] M. Ahn, Y. Park, S. H. Lee, S. Chae, J. Lee, J. T. Heron, E. Kioupakis, W. D. Lu, J. D. Phillips, *Adv. Electron. Mater.* **2021**, *7*, 2001258.
[34] C. Wang, C. Wang, F. Meng, P. Wang, S. Wang, S. Liang, F. Miao, *Adv. Electron. Mater.* **2020**, *6*, 1901107.
[35] T. Wang, Z. He, H. Liu, L. Chen, H. Zhu, Q. Sun, S. Ding, P. Zhou, D. W. Zhang, *ACS Appl. Mater. Interfaces* **2018**, *10*, 37345.

[36] Z. Wang, S. Joshi, S. Savel'ev, W. Song, R. Midya, Y. N. Li, M. Rao, P. Yan, S. Asapu, Y. Zhuo, H. Jiang, P. Lin, C. Li, J. H. Yoon, N. K. Upadhyay, J. Zhang, M. Hu, J. P. Strachan, M. Barnell, Q. Wu, H. Wu, R. S. Williams, Q. Xia, J. J. Yang, *Nat. Electron.* **2018**, *1*, 137.
[37] Y. Lecun, L. Bottou, Y. Bengio, P. Haffner, *Proc. IEEE* **1998**, *86*, 2278.
[38] S. Ham, S. Choi, H. Cho, S. I. Na, G. Wang, *Adv. Funct. Mater.* **2019**, *29*, 1806646.
[39] Z. Lv, M. Chen, F. Qian, V. A. L. Roy, W. Ye, D. She, Y. Wang, Z. Xu, Y. Zhou, S. Han, *Adv. Funct. Mater.* **2019**, *29*, 1902374.
[40] X. Xu, S. Xie, Y. Zhang, H. Peng, *Angew. Chem., Int. Ed.* **2019**, *58*, 13643.
[41] A. Y. Hannun, P. Rajpurkar, M. Haghpanahi, G. H. Tison, C. Bourn, M. P. Turakhia, A. Y. Ng, *Nat. Med.* **2019**, *25*, 65.
[42] S. Singh, S. K. Pandey, U. Pawar, R. R. Janghel, *Procedia Comput. Sci.* **2018**, *132*, 1290.
[43] E. Essa, X. Xie, *IEEE Access* **2021**, *9*, 103452.
[44] C. Yang, D. Shang, N. Liu, E. J. Fuller, S. Agrawal, A. A. Talin, Y. Li, B. Shen, Y. Sun, *Adv. Funct. Mater.* **2018**, *28*, 1804170.